

Density functional study of orbital-selective magnetism in FeAs-based superconductors

Hyungju Oh, Donghan Shin, and Hyoung Joon Choi*
Department of Physics and IPAP, Yonsei University, Seoul 120-749, Korea
(Dated: March 9, 2018)

We performed spin-polarized density functional calculations of lanthanide-series (Ln) iron oxypnictides LnFeAsO (Ln=La, Ce, Pr, Nd, Sm, and Gd) with constrained Fe magnetic moments, finding that in-plane d_{xy} and out-of-plane d_{yz} orbital characters are preferred for small Fe magnetic moments. Comparison of LnFeAsO compounds shows that the antiferromagnetism (AFM) from the Fe d_{xy} orbital is itinerantly driven by orbital-dependent Fermi-surface nesting while AFM from the Fe d_{yz} orbital is driven by superexchange mechanism. The Fe magnetic moments of the two orbital characters show different coupling strengths to Fermi-surface electrons orbital-selectively, suggesting that they may play different roles in superconductivity and in AFM, and making d orbital characters of the magnetic moment resolvable by measuring the electronic structures.

PACS numbers: 71.15.Mb, 71.20.-b, 74.70.Xa, 75.25.-j

$\text{LaFeAsO}_{1-x}\text{F}_x$ (Ref. 1) and related compounds show unconventional superconductivity (SC) in the vicinity of antiferromagnetism (AFM).²⁻¹⁶ Among various families of iron pnictides and chalcogenides, lanthanide-series (Ln) iron oxypnictides LnFeAsO show the highest superconducting transition temperature (T_c) with doping. Reported T_c in doped LnFeAsO increases dramatically from 26 K up to 55 K with Nd or Sm substitution for La and then T_c decreases slightly in doped GdFeAsO .^{1,2,8,11-15} With this strong variation of T_c , LnFeAsO is suited for studying material dependence of T_c .¹⁷ Since FeAs-based materials are featured with multiple Fermi surfaces (FSs) with strong orbital characters, many theoretical and experimental studies have been done on FS nesting, local-moment interactions, and orbital orderings.¹⁷⁻²⁸

So far, study of orbital physics in FeAs-based materials is focused mainly on d_{yz} versus d_{zx} orbital characters.^{23,24,29-31} It was claimed theoretically that Fe d_{yz} orbital is less occupied but more spin-polarized than Fe d_{zx} orbital, resulting in ferro-orbital order.^{23,24,29} It was also claimed theoretically that the low-energy orbital polarization between d_{yz} and d_{zx} orbitals leads to the anisotropy of the optical conductivity.³⁰ The orbital magnetization was reported to be far stronger for the d_{yz} orbital than it is for d_{zx} , which suggests that the orbital degree of freedom strongly couples to the magnetic order.³¹ All these works are focused on comparing Fe d_{yz} and d_{zx} orbitals and indicate that d_{yz} orbital has more important roles in magnetism or orbital order than d_{zx} orbital does, not considering any possible role of the other d orbitals. However, it was reported, for example, that Fe d_{xy} orbital contributes more to Fe magnetic moment than d_{zx} orbital does.³² Thus, full analysis of orbital characters including d_{xy} orbital is needed for electronic and magnetic properties of FeAs-based materials.

In this paper, we report spin-polarized density functional calculations of LnFeAsO (Ln=La, Ce, Pr, Nd, Sm, and Gd), constraining the magnitude and the d orbital character of Fe magnetic moment. We find that in-plane d_{xy} and out-of-plane d_{yz} orbital characters are energetically

ically preferred for Fe magnetic moments when the moments are small and ordered antiferromagnetically along the x direction and ferromagnetically along the y direction. Comparison of atomic and electronic structures of LnFeAsO compounds shows that AFM from the Fe d_{xy} orbital is itinerantly driven by orbital-dependent FS nesting while AFM from the Fe d_{yz} orbital is driven by superexchange mechanism. The Fe magnetic moments of the two orbital characters show different coupling strengths to FS electrons orbital-selectively. This suggests that Fe moments of different orbital character can be resolved by measuring the electronic structures and may have different role in SC and AFM.

Our calculations are based on *ab-initio* norm-conserving pseudopotentials and the Perdew-Burke-Ernzerhof-type generalized gradient approximation to the density functional theory (DFT), as implemented in the SIESTA code.³³ Electronic wavefunctions are expanded with pseudoatomic orbitals (double- ζ polarization), which yields orbital characters in electronic and magnetic properties straightforwardly. In our present work, the size of the magnetic moment (m_{Fe}) of a Fe atom is defined as the difference of spin-up and spin-down electrons occupying pseudoatomic orbitals of the Fe atom. During self-consistent iterations, the total-energy functional is minimized with constraints imposed on the electron spin density in order to control the size and the orbital character of the Fe magnetic moment. Since experimentally reported values of the Fe magnetic moment in LnFeAsO are quite smaller than the unconstrained DFT values of the Fe magnetic moment, we consider constraining the size of the Fe magnetic moment to a quite smaller value than an unconstrained one. To consider a Fe magnetic moment of a specific d -orbital character, constraints are imposed so that only a specified d orbital can have different occupations of spin-up and spin-down electrons while all the other d orbitals are spin-unpolarized. We assume an oxidation state of +3 for all considered Ln elements, treating their $4f$ orbitals as core orbitals.^{34,35} Experimental lattice constants and atomic positions at

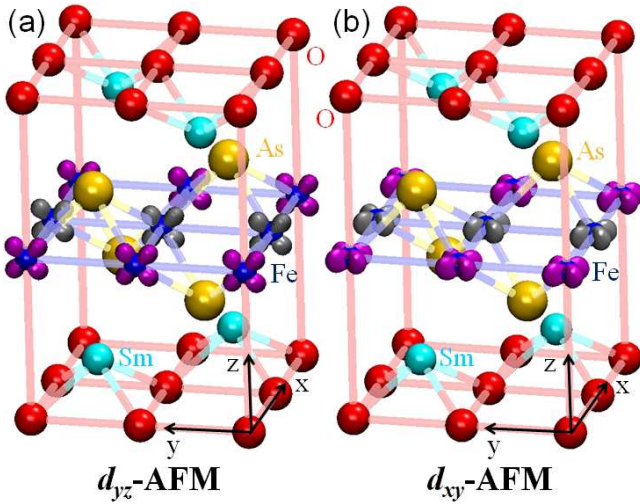


FIG. 1. (Color online) Orbital characters of Fe magnetic moments in SmFeAsO: (a) d_{yz} -AFM where Fe magnetic moments have only d_{yz} orbital character and (b) d_{xy} -AFM where Fe magnetic moments have only d_{xy} orbital character. In (a) and (b), the size of each Fe magnetic moment (m_{Fe}) is constrained to $0.10 \mu_{\text{B}}$ as an example of small m_{Fe} . Each atomic structure is a $\sqrt{2} \times \sqrt{2} \times 1$ supercell with four Fe atoms in the single-stripe-type AFM. Fe magnetic moments, in dark and light gray (purple and light gray) which represent opposite directions of the moments, are ordered antiferromagnetically along the x axis and ferromagnetically along the y axis. In (a) and (b), the d orbital shapes of Fe magnetic moments contain 50% of the total spin density. The example value of m_{Fe} of $0.10 \mu_{\text{B}}$ is about 30% of the experimental value of $0.34 \mu_{\text{B}}$ in SmFeAsO.¹⁴

the high-temperature tetragonal phase^{3,4,9,10,15,36,37} are used in our calculations in order to focus on effects of Fe magnetic moments on the electronic and magnetic properties³⁸ although LnFeAsO is orthorhombic at low temperature. A dense \mathbf{k} -point grid of $32 \times 32 \times 32$ is used to determine the Fermi energy (E_{F}) and FS properties precisely. Spin-orbit coupling is not considered, since our separate test calculations show that spin-orbit coupling has only minor effects on properties under consideration in our present work.

An intriguing finding in our present calculations is distinctive d -orbital characters of the Fe magnetic moment in LnFeAsO in small m_{Fe} regime. Figure 1 shows two prototypical cases of SmFeAsO in the single-stripe-type AFM with antiferromagnetic ordering along the x direction and ferromagnetic ordering along the y direction. When m_{Fe} is set to $0.10 \mu_{\text{B}}$ per Fe atom as an example of small m_{Fe} , SmFeAsO has two almost degenerate ground states. In one case [Fig. 1(a)] the Fe magnetic moment has out-of-plane d_{yz} orbital character while in the other case [Fig. 1(b)] the Fe magnetic moment has in-plane d_{xy} orbital character. In the former case the Fe magnetic moment is made by spin polarization of electrons in d_{yz} orbitals while in the latter case the Fe magnetic moment is made by spin polarization of

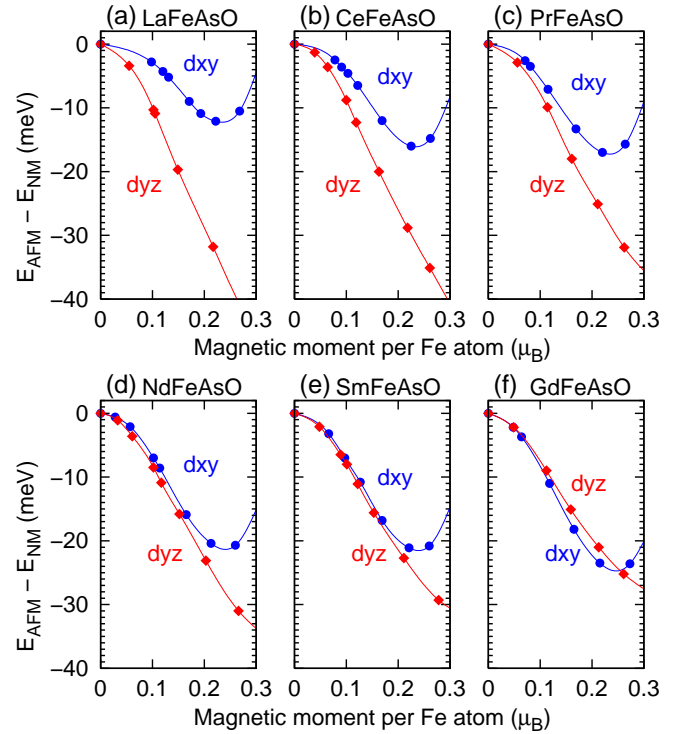


FIG. 2. (Color online) The total energy of LnFeAsO in d_{xy} - and d_{yz} -AFMs with constrained Fe magnetic moments: (a) LaFeAsO, (b) CeFeAsO, (c) PrFeAsO, (d) NdFeAsO, (e) SmFeAsO, and (f) GdFeAsO. The total energy per supercell containing four Fe atoms is plotted as a function of the magnetic moment per Fe atom. Fe magnetic moments are constrained to specific values and to either d_{xy} or d_{yz} orbital character. In each plot, the total energy of the nonmagnetic phase is set to zero.

electrons in d_{xy} orbitals. When we considered Fe magnetic moments having d -orbital characters other than d_{yz} and d_{xy} , we obtained the total energy which is higher than the nonmagnetic case, so we consider only d_{yz} and d_{xy} orbital characters for the Fe magnetic moment in our present work. In previous studies, the main concern was not d_{yz} versus d_{xy} orbitals, but d_{yz} versus d_{zx} orbitals in regard to symmetry lowering from tetragonal to orthorhombic structures. In our present work, symmetry is lowered by imposing the single-stripe-type AFM and then either d_{yz} or d_{xy} orbital character is found predominant in the Fe magnetic moment, interestingly.

For systematic study, we calculated the total energy of LnFeAsO in the single-stripe-type AFM with Fe magnetic moments constrained to have either d_{yz} or d_{xy} orbital character (which we denote as d_{yz} -AFM and d_{xy} -AFM, respectively) as a function of m_{Fe} , as shown in Fig. 2. With Ln ranging from La to Gd, we found that d_{yz} -AFM becomes less and less stable while d_{xy} -AFM becomes more and more stable. In LaFeAsO, d_{yz} -AFM is lower in energy than d_{xy} -AFM with the total-energy difference of about 20 meV per four Fe atoms when m_{Fe} is $0.20 \mu_{\text{B}}$, as shown in Fig. 2(a). However, in the case

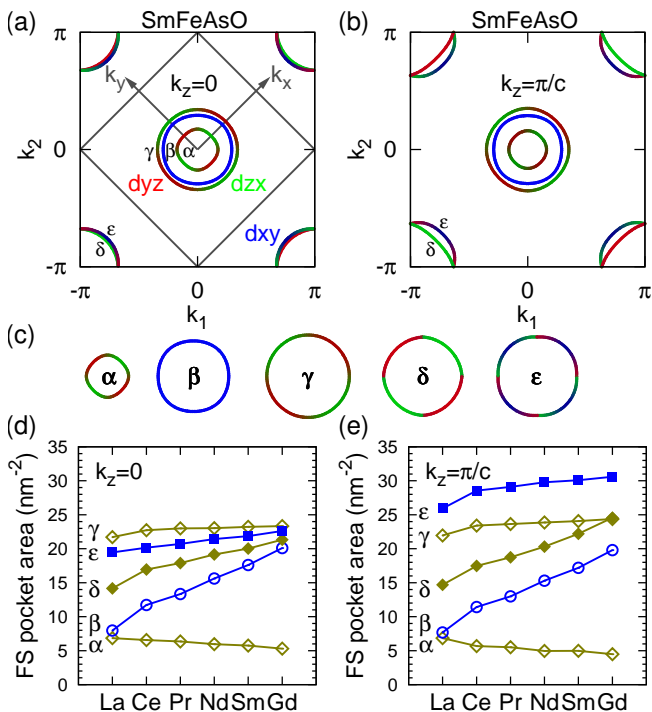


FIG. 3. (Color online) Orbital characters and pocket areas of Fermi surfaces (FSs) in nonmagnetic LnFeAsO. (a) FS of nonmagnetic SmFeAsO at $k_z = 0$ and (b) at $k_z = \pi/c$. The k_1 and k_2 axes are along reciprocal lattice vectors of the nonmagnetic unit cell having two Fe atoms. In (a), the 45°-rotated inner square is the first Brillouin zone of the $\sqrt{2} \times \sqrt{2} \times 1$ supercell having four Fe atoms, where k_x and k_y axes are along the x and y axes in Fig. 1(a), respectively. Three hole pockets (α , β , and γ) are located at the center and two electron pockets (δ and ϵ) at the corner. Orbital characters, d_{xy} , d_{yz} , and d_{zx} , are represented in blue, red, and green, respectively. The α , γ , and δ pockets are derived from d_{yz} and d_{zx} , the β pocket is from d_{xy} , and the ϵ pocket is from d_{xy} , d_{yz} , and d_{zx} . (c) FS pockets at $k_z = 0$. The δ and ϵ pockets are plotted as closed loops to highlight changes in orbital characters around the pockets. (d) Areas of the five FS pockets at $k_z = 0$ and (e) at $k_z = \pi/c$ as a function of Ln elements.

of SmFeAsO, d_{xy} - and d_{yz} -AFMs are nearly degenerate when m_{Fe} is less than $0.20 \mu_B$, as shown in Fig. 2(e). In GdFeAsO, d_{xy} -AFM has a lower total energy than d_{yz} -AFM, so d_{xy} -AFM becomes dominant [Fig. 2(f)].

Our additional calculation of PrFeAsO in NdFeAsO structure shows that it has the same orbital features as NdFeAsO, indicating that the major role of different Ln atoms is to change structural parameters. Thus the Ln-dependent gradual change of the total energy of d_{yz} - and d_{xy} -AFMs, shown in Fig. 2, is mainly from the change in structural parameters including the As height from the Fe plane. Considering overall increase of measured T_c in doped LnFeAsO from La to Gd,^{1,2,8,11-15} the different Ln-dependences of the calculated total energy in the d_{yz} - and d_{xy} -AFMs suggest that electrons in Fe d_{yz} and d_{xy} orbitals may play different roles in SC.

To understand the origin of the distinctive orbital char-

acters of the Fe magnetic moments, we analyzed orbital characters of electronic states at the Fermi energy in nonmagnetic LnFeAsO. As a prototype, SmFeAsO has three cylindrical hole-type FS pockets [α , β , and γ pockets in Figs. 3(a)-(c)] and two electron-type FS pockets [δ and ϵ pockets in Figs. 3(a)-(c)] at E_F . Orbital analysis shows that the α , γ , and δ pockets are derived from Fe d_{yz} and d_{zx} orbitals, the β pocket is from d_{xy} , and the ϵ pocket is from d_{xy} , d_{yz} , and d_{zx} [Figs. 3(a)-(c)]. For FS nesting, we consider six pairs of hole and electron pockets: α - δ , β - δ , γ - δ , α - ϵ , β - ϵ , and γ - ϵ pairs. Among these, α - δ nesting is not significant because the two pockets have quite different pocket areas in all LnFeAsO [Figs. 3(d) and (e)], and β - δ nesting is not effective because orbital difference of the two pockets degrades effects of nesting greatly. In addition, γ - δ and α - ϵ nesting effects should be very weak because of orbital mismatch due to out-of-phase alternations of d_{yz} and d_{zx} characters around the pockets. Thus, we need to examine only β - ϵ and γ - ϵ nesting.

As mentioned above, the β -hole pocket in LnFeAsO [Figs. 3(a)-(c)] is derived from the d_{xy} orbital, the γ -hole pocket is from d_{yz} and d_{zx} orbitals, and the ϵ -electron pocket is from d_{xy} , d_{yz} , and d_{zx} orbitals. Thus we need to analyze whether the β - ϵ nesting is related with d_{xy} orbital character of the Fe magnetic moment and whether the γ - ϵ nesting is related with d_{yz} or d_{zx} orbital character of the moment. Calculated FS pocket areas in LnFeAsO [Figs. 3(d) and (e)] show that the β -hole pocket area depends sensitively on Ln elements and it is closer to the ϵ -electron pocket area for heavier Ln elements, implying that β - ϵ nesting is better for heavier Ln elements. Considering the increase of stability of d_{xy} -AFM from La to Gd [Fig. 2], we find that the FS nesting between the β and ϵ pockets in LnFeAsO has positive correlation with the d_{xy} orbital character of the Fe magnetic moment. On the contrary, the γ -hole pocket area is almost insensitive to Ln elements and close to the ϵ -electron pocket area [Figs. 3(d) and (e)], indicating that the γ - ϵ nesting is good for all LnFeAsO. Considering the decrease of stability of d_{yz} -AFM from La to Gd [Fig. 2], we conclude that the FS nesting between the γ and ϵ pockets in LnFeAsO is hardly related with the d_{yz} orbital character of the Fe magnetic moment.

Although it is not involved in the FS nesting, the area of the δ -electron FS pocket, which is derived from d_{yz} and d_{zx} orbitals, also depends sensitively on Ln elements [Figs. 3(d) and (e)]. With heavier Ln elements, the area of the δ -electron pocket increases and so does the area of the β -hole pocket which is derived from the d_{xy} orbital.³⁹ This results in electron transfer from the d_{xy} orbital to the d_{yz} and d_{zx} orbitals. Since the δ -pocket is not related with FS nesting, the increased d_{yz} and d_{zx} electrons in the δ -pocket can contribute to AFM only by Heisenberg-type local-moment interactions.^{7,16} The overall decrease of stability of d_{yz} -AFM from LaFeAsO to GdFeAsO can be understood by the superexchange mechanism. For d_{yz} orbitals of nearest-neighboring Fe atoms, it is known that

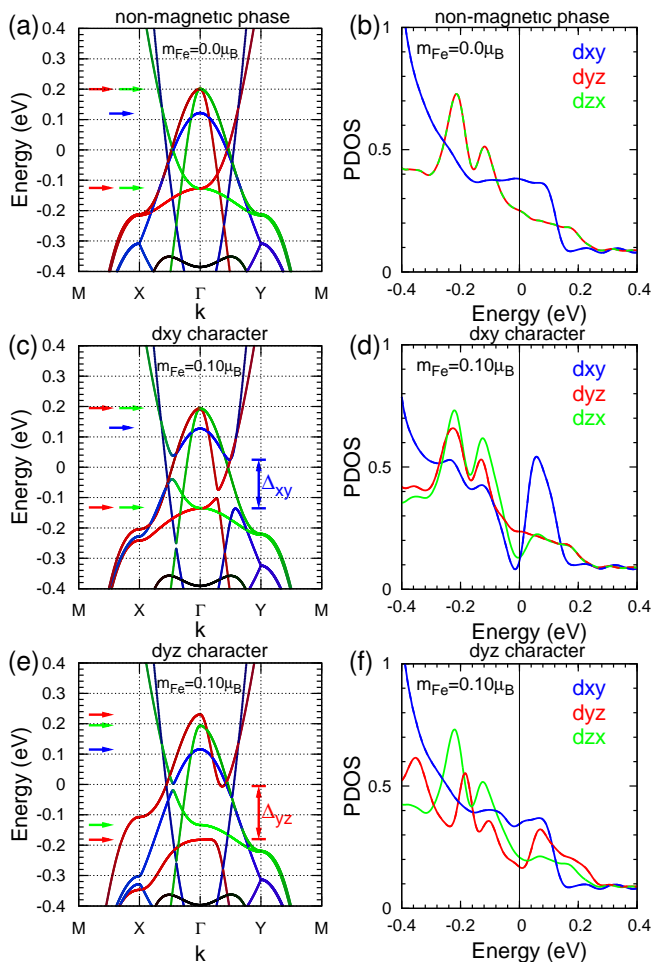


FIG. 4. (Color online) Orbital-resolved electronic band structures and projected density of state (PDOS) in SmFeAsO: (a) and (b) for nonmagnetic phase, (c) and (d) for the d_{xy} -AFM with $m_{\text{Fe}} = 0.10 \mu_{\text{B}}$, and (e) and (f) for the d_{yz} -AFM with $m_{\text{Fe}} = 0.10 \mu_{\text{B}}$. Band structures are plotted along high-symmetry lines in the first Brillouin zone of the $\sqrt{2} \times \sqrt{2} \times 1$ supercell for the single-stripe-type AFM, where M = (0, π), X = ($\pi/2$, $\pi/2$), Γ = (0, 0), and Y = ($-\pi/2$, $\pi/2$) with respect to the unit-cell reciprocal axes, k_1 and k_2 , shown in Fig. 3(a). Blue, red, and green represent d_{xy} , d_{yz} , and d_{zx} orbital characters, respectively, and E_F is set to zero. Horizontal arrows indicate extreme band energies at Γ . In (c), Δ_{xy} indicates energy gap between d_{xy} bands in the ΓY line. In (e), Δ_{yz} indicates energy gap between d_{yz} bands in the ΓY line.

indirect hopping through As p orbitals is larger than direct hopping.^{40–42} From La to Gd, the As height from the Fe plane increases, so the Fe-As-Fe angle decreases, reducing the indirect hopping and thereby weakening the strength of Fe magnetic moment of the d_{yz} orbital character. Thus, the stability of AFM from the Fe d_{yz} orbital is consistent with the Heisenberg-type local-moment interaction due to the superexchange mechanism.

To find out effects of different orbital characters of Fe magnetic moments on the electronic structures, we obtained orbital-resolved band structures and projected

density of states (PDOS) in SmFeAsO, as a prototype of LnFeAsO, in nonmagnetic phase and d_{xy} - and d_{yz} -AFMs (Fig. 4). In the nonmagnetic phase with zero m_{Fe} , energy bands have distinct orbital characters along high-symmetry lines, yielding PDOS slowly varying near E_F [Figs. 4(a) and (b)].

In SmFeAsO in d_{xy} -AFM where Fe magnetic moment has only d_{xy} orbital character, strong anti-crossing occurs between d_{xy} bands, opening orbital-dependent energy gaps at E_F [Fig. 4(c)]. In the ΓX line, d_{xy} and d_{zx} bands repel each other at E_F and at -260 meV. In the ΓY line, d_{xy} bands open a significant energy gap near E_F [marked with Δ_{xy} in Fig. 4(c)], while d_{zx} bands are intact. Except for anti-crossing at -100 meV in the ΓY line, d_{yz} bands are almost unchanged. The d_{xy} PDOS is greatly modified with a partial-gap opening at E_F and a huge peak right above E_F [Fig. 4(d)]. The d_{zx} PDOS also shows a reduction near E_F because of coupling to d_{xy} bands [Fig. 4(d)]. Despite these significant effects on the electronic structures near E_F , deformation of bands is mostly confined near the band-crossing points, with no shift of original band edges [Fig. 4(c)]. This confirms that the Fe magnetic moment of d_{xy} orbital character is due to FS nesting.

In contrast, in SmFeAsO in d_{yz} -AFM where the Fe magnetic moment has only d_{yz} orbital character, d_{yz} bands are deformed in the whole Brillouin zone rather than just anti-crossing of bands [Fig. 4(e)]. Whole upper part of d_{yz} bands and whole lower part of d_{yz} bands are repelled from each other [Fig. 4(e)], so even the top of the hole-type d_{yz} band is pushed up by 40 meV and the bottom of the electron-type d_{yz} band is pushed down by 50 meV. This change of d_{yz} bands in the whole Brillouin zone indicates that the driving mechanism for the d_{yz} orbital character of Fe magnetic moment is not FS nesting which is local in k -space but it is the lowering of the total energy of the electron system by formation of magnetic moments which are local in real space. Despite the significant change in the d_{yz} bands, all the other bands are almost unchanged except for some anti-crossings.

As shown in Fig. 4, Fe magnetic moments with different orbital characters couple differently to electrons at the Fermi energy, so they may have different roles in SC and AFM. In particular, detailed comparison of our band structures with experimental results, e.g., angle-resolved photoemission spectroscopy of detwinned samples,^{28,43} will reveal orbital characters of the Fe magnetic moment, and thereby their roles in AFM. In addition, when m_{Fe} is increased to 1.0 μ_{B} or larger, the Fe magnetic moment evolves gradually to an almost spherical shape with no specific orbital characters. Thus, the orbital-distinctive magnetic moments and their effects will appear with different strengths in various iron pnictides and chalcogenides depending on the wide range of reported m_{Fe} .

In conclusion, we have found that Fe magnetic moment in LnFeAsO (Ln = La to Gd) has distinctive orbital character, d_{xy} or d_{yz} , when the Fe magnetic moment is small

and ordered antiferromagnetically along the x direction and ferromagnetically along the y direction. By comparing atomic structures and calculated d -orbital-resolved electronic structures of the compounds, we have shown that the origins of the d_{xy} and d_{yz} orbital characters of the Fe magnetic moment are orbital-dependent FS nesting and superexchange interactions, respectively. Fe magnetic moments of d_{xy} and d_{yz} orbital characters are

found to have different coupling strengths to electronic states near the Fermi energy, so they can be identified by d -orbital-resolved measurement of electronic structures and they may have different roles in SC and AFM.

This work was supported by the NRF of Korea (Grant Nos. 2009-0081204 and 2011-0018306). Computational resources have been provided by KISTI Supercomputing Center (Project No. KSC-2008-S02-0004).

-
- * Email: h.j.choi@yonsei.ac.kr
- ¹ Y. Kamihara, T. Watanabe, M. Hirano, and H. Hosono, *J. Am. Chem. Soc.* **130**, 3296 (2008).
 - ² X. H. Chen, T. Wu, G. Wu, R. H. Liu, H. Chen, and D. F. Fang, *Nature (London)* **453**, 761 (2008).
 - ³ C. de la Cruz, Q. Huang, J. W. Lynn, J. Li, W. Ratcliff II, J. L. Zarestky, H. A. Mook, G. F. Chen, J. L. Luo, N. L. Wang, and P. Dai, *Nature (London)* **453**, 899 (2008).
 - ⁴ J. Zhao, Q. Huang, C. de la Cruz, S. Li, J. W. Lynn, Y. Chen, M. A. Green, G. F. Chen, G. Li, Z. Li, J. L. Luo, N. L. Wang, and P. Dai, *Nature Materials* **7**, 953 (2008).
 - ⁵ Z. P. Yin, S. Lebègue, M. J. Han, B. P. Neal, S. Y. Savrasov, and W. E. Pickett, *Phys. Rev. Lett.* **101**, 047001 (2008).
 - ⁶ I. I. Mazin, D. J. Singh, M. D. Johannes, and M. H. Du, *Phys. Rev. Lett.* **101**, 057003 (2008).
 - ⁷ T. Yildirim, *Phys. Rev. Lett.* **101**, 057010 (2008).
 - ⁸ G. F. Chen, Z. Li, D. Wu, G. Li, W. Z. Hu, J. Dong, P. Zheng, J. L. Luo, and N. L. Wang, *Phys. Rev. Lett.* **100**, 247002 (2008).
 - ⁹ Y. Qiu, W. Bao, Q. Huang, T. Yildirim, J. M. Simmons, M. A. Green, J. W. Lynn, Y. C. Gasparovic, J. Li, T. Wu, G. Wu, and X. H. Chen, *Phys. Rev. Lett.* **101**, 257002 (2008).
 - ¹⁰ J. Zhao, Q. Huang, C. de la Cruz, J. W. Lynn, M. D. Lumsden, Z. A. Ren, J. Yang, X. Shen, X. Dong, Z. Zhao, and P. Dai, *Phys. Rev. B* **78**, 132504 (2008).
 - ¹¹ Z. A. Ren, J. Yang, W. Lu, W. Yi, G. C. Che, X. L. Dong, L. L. Sun, and Z. X. Zhao, *Mater. Res. Innov.* **12**, 105 (2008).
 - ¹² Z. Ren, W. Lu, J. Yang, W. Yi, X. Shen, Z. Li, G. Che, X. Dong, L. Sun, F. Zhou, and Z. Zhao, *Chin. Phys. Lett.* **25**, 2215 (2008).
 - ¹³ K. Miyazawa, K. Kihou, P. M. Shirage, C. Lee, H. Kito, H. Eisaki, and A. Iyo, *J. Phys. Soc. Jpn.* **78**, 034712 (2009).
 - ¹⁴ Y. Kamihara, T. Nomura, M. Hirano, J. E. Kim, K. Kato, M. Takata, Y. Kobayashi, S. Kitao, S. Higashitaniguchi, Y. Yoda, M. Seto, and H. Hosono, *New J. Phys.* **12**, 033005 (2010).
 - ¹⁵ P. Wang, Z. M. Stadnik, C. Wang, G. Cao, and Z. Xu, *J. Phys. Condens. Matter* **22**, 145701 (2010).
 - ¹⁶ C. Y. Moon and H. J. Choi, *Phys. Rev. Lett.* **104**, 057003 (2010).
 - ¹⁷ K. Kuroki, H. Usui, S. Onari, R. Arita, and H. Aoki, *Phys. Rev. B* **79**, 224511 (2009).
 - ¹⁸ S. Lebègue, *Phys. Rev. B* **75**, 035110 (2007).
 - ¹⁹ D. H. Lu, M. Yi, S. K. Mo, A. S. Erickson, J. Analytis, J. H. Chu, D. J. Singh, Z. Hussain, T. H. Geballe, I. R. Fisher, and Z. X. Shen, *Nature (London)* **455**, 81 (2008).
 - ²⁰ D. J. Singh and M. H. Du, *Phys. Rev. Lett.* **100**, 237003 (2008).
 - ²¹ K. Haule, J. H. Shim, and G. Kotliar, *Phys. Rev. Lett.* **100**, 226402 (2008).
 - ²² C.-Y. Moon, S. Y. Park, and H. J. Choi, *Phys. Rev. B* **78**, 212507 (2008).
 - ²³ C.-C. Lee, W.-G. Yin, and W. Ku, *Phys. Rev. Lett.* **103**, 267001 (2009).
 - ²⁴ F. Krüger, S. Kumar, J. Zaanen, and J. van den Brink, *Phys. Rev. B* **79**, 054504 (2009).
 - ²⁵ C.-Y. Moon, S. Y. Park, and H. J. Choi, *Phys. Rev. B* **80**, 054522 (2009).
 - ²⁶ C. C. Chen, J. Maciejko, A. P. Sorini, B. Moritz, R. R. P. Singh, and, T. P. Devereaux, *Phys. Rev. B* **82**, 100504(R) (2010).
 - ²⁷ W. Lv, F. Krüger, and P. Phillips, *Phys. Rev. B* **82**, 045125 (2010).
 - ²⁸ M. Yi, D. Lu, J. Chu, J. G. Analytis, A. P. Sorini, A. F. Kemper, B. Moritz, S. Mo, R. G. Moore, M. Hashimoto, W. Lee, Z. Hussain, T. P. Devereaux, I. R. Fisher, and Z. X. Shen, *Proc. Natl. Acad. Sci. USA* **108**, 6878 (2011).
 - ²⁹ W. Lv, J. Wu, and P. Phillips, *Phys. Rev. B* **80**, 224506 (2009).
 - ³⁰ Z. P. Yin, K. Haule, and G. Kotliar, *Nature Physics* **7**, 294 (2011).
 - ³¹ M. Daghofer, Q.-L. Luo, R. Yu, D. X. Yao, A. Moreo, and E. Dagotto, *Phys. Rev. B* **81**, 180514(R) (2010).
 - ³² Z. P. Yin and W. E. Pickett, *Phys. Rev. B* **81**, 174534 (2010).
 - ³³ D. Sánchez-Portal, P. Ordejón, E. Artacho, and J. M. Soler, *Int. J. Quantum Chem.* **65**, 453 (1997).
 - ³⁴ I. A. Nekrasov, Z. V. Pchelkina, and M. V. Sadovskii, *JETP Letters* **87**, 560 (2008).
 - ³⁵ L. Pourovskii, V. Vildosola, S. Biermann, and A. Georges, *Europhys. Lett.* **84**, 37006 (2008).
 - ³⁶ A. Martinelli, A. Palenzona, C. Ferdeghini, M. Putti, and H. Emerich, *J. Alloys Comp.* **477**, L21 (2009).
 - ³⁷ While our spin-unpolarized calculation predicts the lattice constants of the nonmagnetic tetragonal phase accurately, it underestimates the As height by 0.1 Å because it neglects non-zero Fe magnetic moment which is actually present even at high-temperature nonmagnetic phase. The As height is predicted correctly by our spin-polarized calculation.
 - ³⁸ Our test calculations show that using an orthorhombic unit cell rather than a tetragonal one produces only a small change in orbital occupation of d_{xz} and d_{yz} , with no significant change in our main results of d_{xy} versus d_{yz} orbital characters.
 - ³⁹ We also calculated Fermi-surface pocket areas in $\text{LnFeAsO}_{0.9}\text{F}_{0.1}$ using the virtual crystal approximation, and found that the F doping does not alter Ln-dependent changes of β - and δ -pocket areas although the F doping

shrinks hole-type pockets and enlarges electron-type pockets compared with undoped cases.

⁴⁰ M. J. Calderón, B. Valenzuela, and E. Bascones, *Phys. Rev. B* **80**, 094531 (2009).

⁴¹ K. Haule and G. Kotliar, *New J. Phys.* **11**, 025021 (2009).

⁴² Z. P. Yin, K. Haule, and G. Kotliar, *Nature Materials* **10**,

932 (2011).

⁴³ Y. Kim, H. Oh, C. Kim, D. Song, W. Jung, B. Kim, H. J. Choi, C. Kim, B. Lee, S. Khim, H. Kim, K. Kim, J. Hong, and Y. Kwon, *Phys. Rev. B* **83**, 064509 (2011).